

Retrograde Plasticity and Differential Competition of Bipolar Cell Dendrites and Axons in the Developing Retina

Robert E. Johnson¹ and Daniel Kerschensteiner^{1,2,3,*}¹Department of Ophthalmology and Visual Sciences²Department of Anatomy and Neurobiology³Hope Center for Neurological Disorders

Washington University School of Medicine, Saint Louis, MO 63110, USA

Summary

Most neurons function in the context of pathways that process and propagate information through a series of stages, e.g., from the sensory periphery to cerebral cortex [1]. Because activity at each stage of a neural pathway depends on connectivity at the preceding one, we hypothesized that during development, axonal output of a neuron may regulate synaptic development of its dendrites (i.e., retrograde plasticity). Within pathways, neurons often receive input from multiple partners and provide output to targets shared with other neurons (i.e., convergence) [2]. Converging axons can intermingle or occupy separate territories on target dendrites. Activity-dependent competition has been shown to bias target innervation by overlapping axons in several systems [3–8]. By contrast, whether territorial axons or dendrites compete for targets and inputs, respectively, has not been tested. Here, we generate transgenic mice in which glutamate release from specific sets of retinal bipolar cells (BCs) is suppressed. We find that dendrites of silenced BCs recruit fewer inputs when their neighbors are active and that dendrites of active BCs recruit more inputs when their neighbors are silenced than either active or silenced BCs with equal neighbors. By contrast, axons of silenced BCs form fewer synapses with their targets, irrespective of the activity of their neighbors. These findings reveal that retrograde plasticity guides BC dendritic development in vivo and demonstrate that dendrites, but not territorial axons, in a convergent neural pathway engage in activity-dependent competition. We propose that at a population level, retrograde plasticity serves to maximize functional representation of inputs.

Results and Discussion

Bipolar cells (BCs) are glutamatergic second-order neurons of the visual system that receive input from photoreceptors (rods or cones) in the outer retina and innervate amacrine (ACs) and ganglion (GCs) cells in the inner retina (Figure 1A) [9]. There are 12 types of BCs in mice: seven depolarize (ON BCs) and five hyperpolarize (OFF BCs) to light increments [9, 10]. Here, we analyze the influence of axonal activity on the development of type 6 ON BCs (B6s). Each B6 receives input from approximately four cones (Figure 2) [11], and approximately 200 of them converge onto a specific GC target [12, 13].

We previously developed mice in which a few B6s in each retina exhibit bright red fluorescence (Figure 1B, *tdTomato*),

as well as mice in which all ON BCs express the light chain of tetanus toxin (Figure 1C, *TeNT*) and yellow fluorescent protein (YFP) [12, 14]. For this study, we generated additional transgenic lines expressing *TeNT* and YFP in a sparse subset of B6s (Figure 1D, *TeNT^{sparse}*). *TeNT* inhibits transmitter release by cleaving vesicle-associated membrane protein 2 (VAMP2) [15]. Immunohistochemistry showed that VAMP2 is depleted similarly in YFP-positive axon terminals of *TeNT* and *TeNT^{sparse}* mice and that YFP-negative ON BC axons in *TeNT^{sparse}* retinas contain normal levels of VAMP2 (Figures 1E–1I). We next compared electroretinographic (ERG) responses of wild-type (*WT*) and *TeNT* mice (Figure 1J). The preserved a-wave amplitudes of *TeNT* mice (Figure 1K) suggest that photoreceptor responses to light are unchanged. Oscillatory potentials and b-waves in the ERG arise in third-order neurons (ACs and GCs) and BCs plus third order neurons, respectively [16]. Accordingly, we interpret the nearly complete suppression of oscillatory potentials (Figure 1M) accompanied by a small reduction in b-wave amplitudes (Figure 1L) in *TeNT* mice as evidence that *TeNT* expression blocks glutamate release from BC axons in vivo, with no or only minor effects on signaling in BC dendrites. In vitro patch clamp and multielectrode array (MEA) recordings from GCs corroborate reduced transmitter release from BCs [14].

To analyze the role of transmitter release in the development of converging territorial axons, we compared arbor morphologies and synapse patterns of active B6 axons with active neighbors (*WT*), silenced B6 axons with silenced neighbors (*TeNT*), and silenced B6 axons with active neighbors (*TeNT^{sparse}*). Individual B6s were visualized either by crossing to *tdTomato* mice (*WT* and *TeNT*) or by YFP expression in *TeNT^{sparse}* mice. Axons of each BC type are strictly territorial and tile the retinal surface with few gaps and little overlap [10]. Confocal reconstructions revealed that B6 axons that are unable to release glutamate establish normal territories, even when surrounded by active neighbors (Figures 2A–2D). Similarly, stratification patterns of B6 axons were indistinguishable between *WT*, *TeNT* and *TeNT^{sparse}* mice (Figure S1), indicating that laminar targeting and territorial interactions of BC axons are independent of transmitter release. We next counted synapses, as identified by punctate labeling for C-terminal binding protein 2 (CtBP2) (Figures 2A–2C), a component of presynaptic ribbons [17], which has been confirmed to appose postsynaptic specializations on GCs and ACs [12, 14, 18, 19]. We found that silenced B6 axons formed fewer synapses (Figure 2E); numbers were equally reduced in *TeNT* and *TeNT^{sparse}* mice, suggesting that neurotransmitter release regulates target innervation by territorial axons without competition [20]. The difference in observations made of overlapping axons [3–8] suggests that the territorial arrangement of axons may serve to constrain the role of activity in synaptic development. We previously observed similar architectural boundaries to the influence of neurotransmission between axons targeting separate layers of bis-tratified dendrites [14].

To test whether neurotransmission retrogradely regulates dendritic development, we reconstructed B6 dendrites—and visualized their contacts with cone terminals by labeling with

*Correspondence: dkerschensteiner@wustl.edu

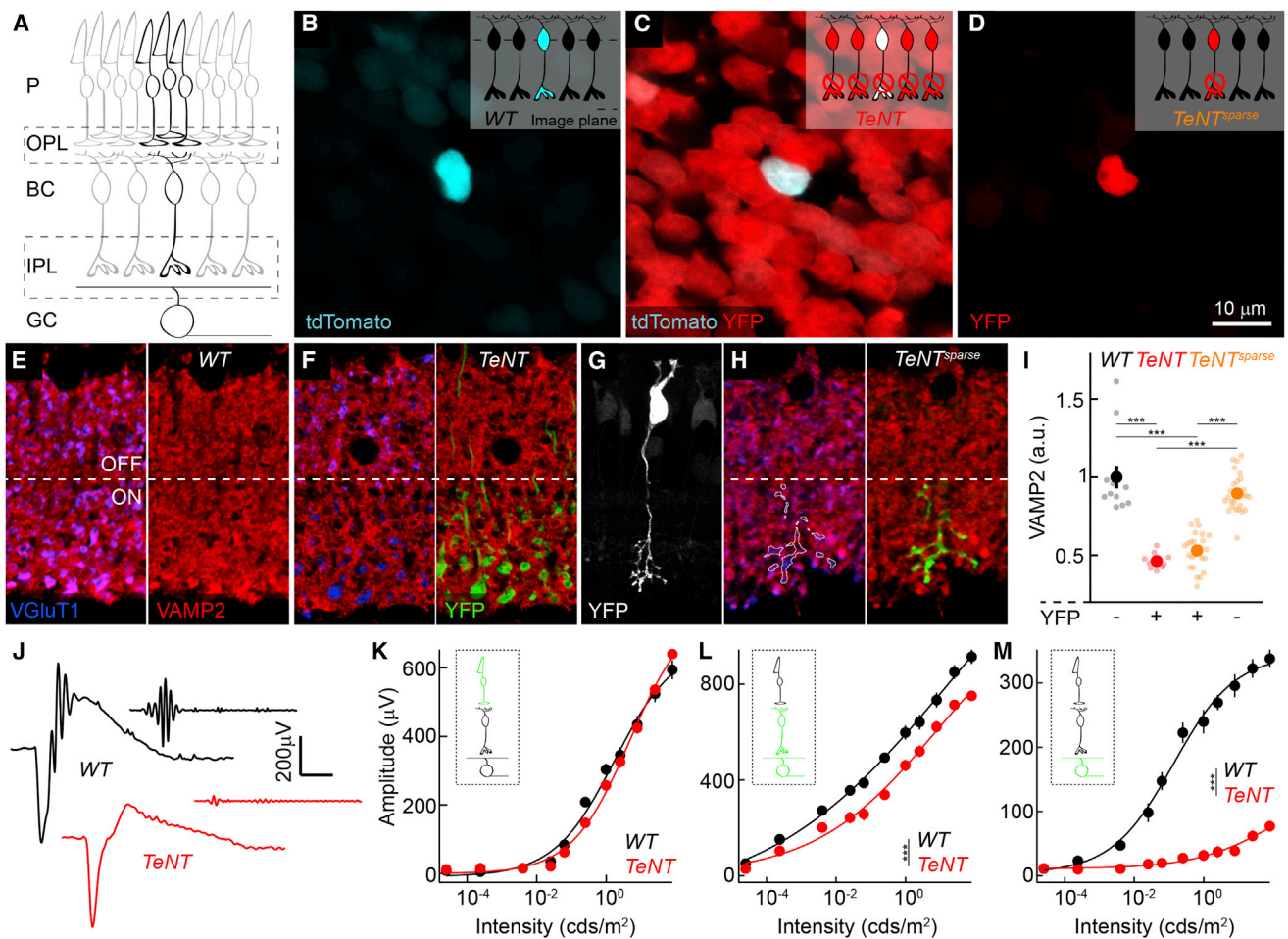


Figure 1. Transgenic Silencing of Specific Sets of Bipolar Cells In Vivo

(A) Schematic of the convergent vertical pathway through the retina. Several photoreceptors (P) synapse onto the dendrites of each bipolar cell (BC) in the outer plexiform layer (OPL). Axons of many BCs in turn innervate each ganglion cell (GC) in the inner plexiform layer (IPL). (B–D) Images of BC somata in flat-mounted retinas illustrate the expression patterns of tdTomato (cyan) and YFP (red, coexpressed with TeNT) in WT (B), TeNT (C), and TeNT^{sparse} (D) mice. Inset schematics illustrate labeling (black, unlabeled; cyan, tdTomato; red, YFP; white, tdTomato and YFP) and activity status of the analyzed B6 cells (middle cell) and their neighbors. Red circles with diagonal crossings indicate axonal silencing by TeNT expression. (E–H) Images of vibratome sections through the IPL of WT (E), TeNT (F), and TeNT^{sparse} (G and H) retinas show VAMP2 depletion in axon terminals (VGlut1) of TeNT-expressing (i.e., YFP-positive) ON BCs. A zoomed-out view of an isolated YFP-positive B6 in a TeNT^{sparse} retina is shown in (G). The left panel of (H) includes an outline of the perimeter of the masked axon terminal of the B6 shown in (G) and the right panel of (H). (I) Quantification of the VAMP2 content of YFP-negative and YFP-positive ON BC axon terminals in WT (n = 12), TeNT (n = 10), and TeNT^{sparse} (n = 26) retinas. Each small circle represents one retinal section, and large circles (error bars) denote population averages (\pm SEM). (J) Raw (lower traces; horizontal scale bar, 50 ms) and high-pass-filtered (cutoff: 100 Hz; upper traces; horizontal scale bar, 66 ms) ERG responses of dark-adapted WT (black) and TeNT (red) retinas to light flashes ($2.526 \text{ cd s m}^{-2}$). (K–M) Population data (WT: n = 5 mice; TeNT: n = 5 mice) of a-wave (K), b-wave (L), and oscillatory potential (M) amplitudes. Insets highlight the cellular origins of the respective ERG components in the vertical pathway in green.

fluorescent peanut agglutinin (PNA)—in WT, TeNT, and TeNT^{sparse} mice (Figures 3A–3C). Importantly, cone densities and terminal sizes were indistinguishable across genotypes (Figure S2). We found that dendrites of active and silenced B6s recruit similar numbers of cones so long as their neighbors are active or silenced as well (WT: 4.15 ± 0.14 , n = 51; TeNT: 4.00 ± 0.21 , n = 27; $p > 0.5$; Figures 3D and S2). By contrast, silenced B6s with active neighbors contact fewer cones (TeNT^{sparse}: 3.31 ± 0.14 , n = 42; $p < 0.0001$ and $p < 0.01$ for comparisons to WT and TeNT, respectively; Figure 3D). These findings suggest that dendrites of neighboring B6s compete for input partners and that the outcome of their competitions is biased by retrograde signals elicited by axonal transmitter release. In WT retinas, the size of synapses on B6 dendrites

decreases with distance from the soma (Figure 3E) as the likelihood of shared cone recruitment by neighboring B6s increases [10, 21]. The absence of this relationship in TeNT-expressing B6s (TeNT and TeNT^{sparse}) further supports the idea that axonal transmitter release influences interactions between dendrites of neighboring BCs (Figures 3F and 3G).

Interestingly, the size of synapses between cones and B6s in TeNT^{sparse} retinas was increased compared to WT and TeNT ($p < 0.0001$ for both comparisons, Figures 3E–3G and S3). We hypothesize that this increase in contact size is a consequence of the decrease in the number of cones contacted, indicative of homeostatic mechanisms that stabilize input to developing BCs. Similar observations of synaptic scaling have previously been made in other circuits [22–24].

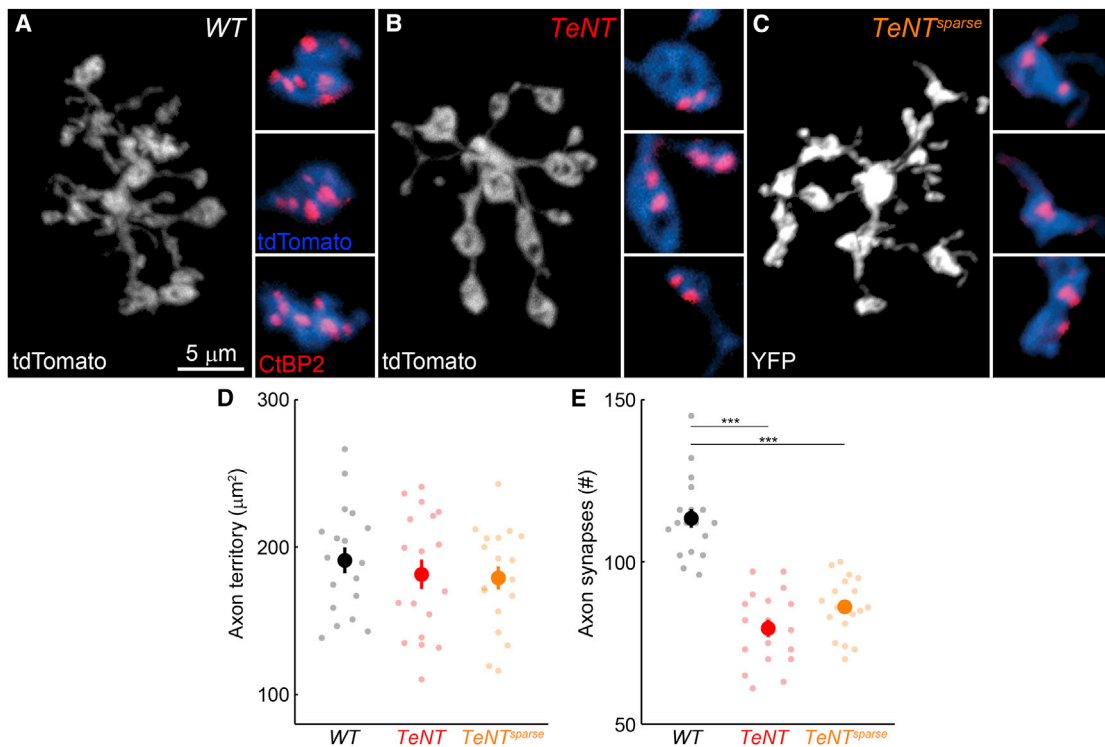


Figure 2. Activity-Dependent Plasticity of BC Axons

(A–C) Projections through confocal image stacks of representative B6 axons in WT (A), *TeNT* (B), and *TeNT^{sparse}* (C) retinas. Insets show single boutons of B6 axons and their CtBP2 labeling.

(D and E) Comparisons of axonal territories (D) and synapse numbers (E) between WT (n = 18), *TeNT* (n = 18), and *TeNT^{sparse}* (n = 19) retinas. Each small circle represents one cell. Large circles (error bars) mark the population averages (±SEM).

See also Figure S1.

If differences in axonal output of neighboring BCs indeed bias the outcome of their dendritic competitions, one would expect that active B6s with silenced neighbors expand dendritic territories and recruit additional cones. To test this prediction, we identified transgenic mice in which 18.5% ± 1.4% of ON BCs express TeNT and YFP distributed in patches of high and low density (Figure 4A, *TeNT^{patchy}*). The patterns of VAMP2 depletion in *TeNT^{patchy}* retinas matched the patterns of YFP expression (Figure S4). Moreover, spatiotemporal receptive fields (RFs) of ON GCs measured in MEA recordings were smaller and spatially less homogeneous in *TeNT^{patchy}* compared to WT retinas but showed preserved kinetics (Figures 4B–4E), suggesting that TeNT-expressing ON BCs are silenced while the remaining ON BCs relay photoreceptor signals to GCs normally. Reconstructions of YFP-negative (i.e., active) B6s surrounded by YFP-positive (i.e., silenced) neighbors in high-density patches (91.8% ± 6.4% YFP-positive ON BCs) of double-transgenic *TeNT^{patchy} tdTomato* retinas (Figure 4A) revealed that their dendrites expand to contact more cones (WT: 4.15 ± 0.14, n = 51; *TeNT^{patchy}*: 5.18 ± 0.21, n = 22; p < 0.001; Figures 4F and 4G), whereas their axons occupy similar territories to WT B6s (WT: 191.02 ± 8.73 μm², n = 18, *TeNT^{patchy}*: 186.25 ± 9.03 μm², n = 19; p > 0.7). The size of cone-B6 contacts was on average slightly increased (p < 0.01), and their centropertipheral gradient across dendritic fields was restored in *TeNT^{patchy}* retinas (Figure 4H). The former suggests that increased input (*TeNT^{patchy}*) during development does not trigger the same homeostatic adjustments as decreased input (*TeNT^{sparse}*), whereas the

latter reflects the influence of axonal activity on dendritic interactions.

Together, our results support the idea that dendrites of developing BCs compete for input partners and that the outcomes of dendritic competitions depend on transmitter release from axons of the same neurons (Figures 4I and 4J). By allocating inputs to developing dendrites of neighboring neurons according to their axon's ability to communicate information onward, retrograde plasticity, at a population level, acts to maximize the functional representation of inputs (i.e., the coverage of inputs whose signals reach target layers). The signals that mediate retrograde influences on dendritic competitions, whether target derived [25] or elicited by actions of glutamate on BCs themselves [26], remain to be identified. Interestingly, modifications of synaptic strength (long-term potentiation and long-term depression) have been shown to back propagate from the *Xenopus* tectum to the retina in a process dependent on BDNF signaling [27].

Unlike input recruitment on dendrites, absolute levels of transmitter release regulate synapse formation of BC axons, rather than differences among neighbors, and axon territories are established independent of activity (Figures 2, 4I, and 4J). Converging territorial axons thus appear to follow different plasticity rules than axons that intermingle on target dendrites, due in part, most likely, to their distinct spatial arrangements [14, 28]. Finally, our findings reveal that dendrites and axons of the same neurons can differentially engage in activity-dependent competitions in vivo, adding further complexity

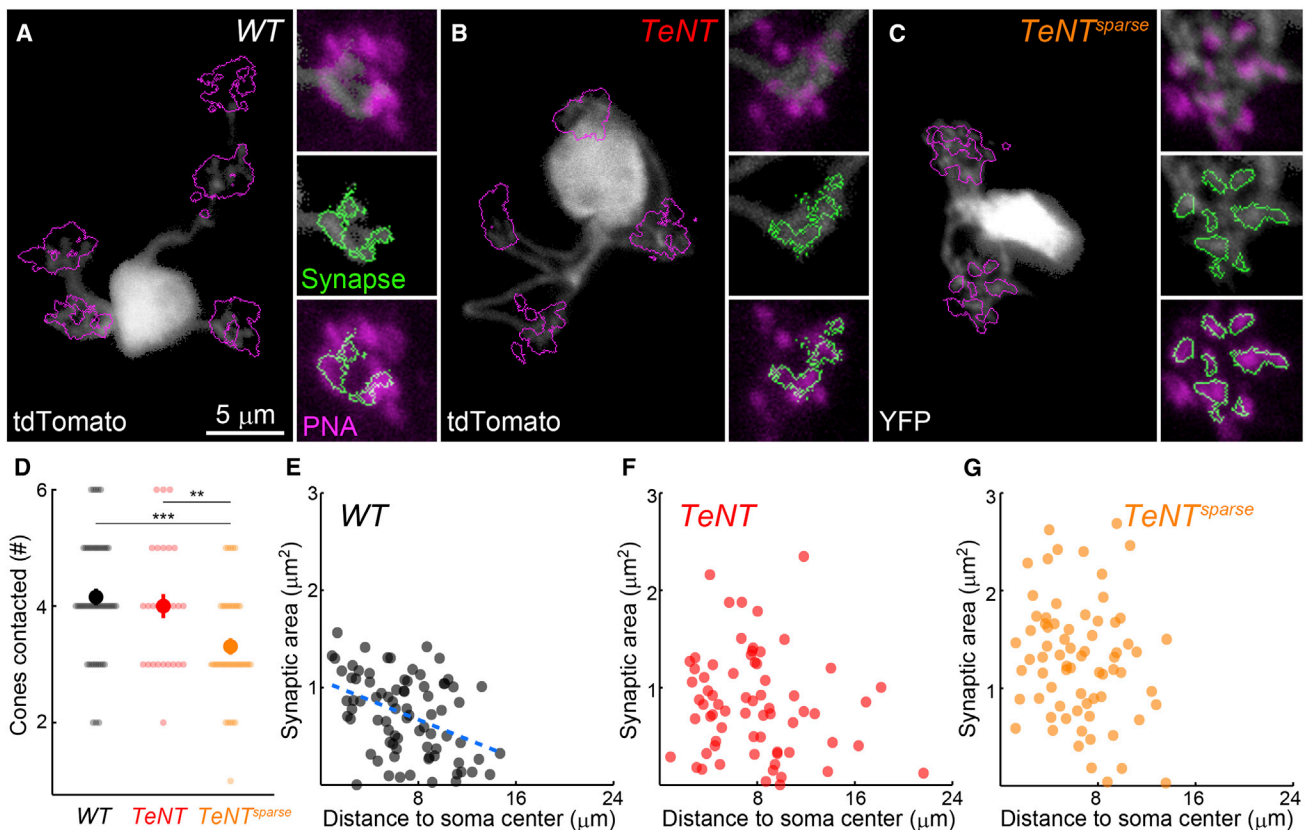


Figure 3. Retrograde Activity-Dependent Plasticity of BC Dendrites

(A–C) Projections through confocal image stacks of representative B6 dendrites in WT (A), TeNT (B), and TeNT^{sparse} (C) retinas. Insets show individual contacts of B6 dendrites and cones stained with fluorescent peanut agglutinin (PNA). The perimeters of cones and synaptic contacts are outlined in magenta and green, respectively.

(D) Summary data comparing the numbers of cones contacted by B6s in WT (n = 51), TeNT (n = 27), and TeNT^{sparse} (n = 42) retinas. Each small circle shows the number of cones contacted by one B6. Large circles (error bars) represent the population averages (\pm SEM).

(E–G) Scatter plots of the area of synaptic contacts between cones and B6 dendrites as a function of distance from the center of the B6 soma. Each circle represents the contacts of one cone with a B6 dendrite (WT: $0.74 \pm 0.05 \mu\text{m}^2$, n = 87; TeNT: $0.88 \pm 0.07 \mu\text{m}^2$, n = 71; TeNT^{sparse}: $1.31 \pm 0.07 \mu\text{m}^2$, n = 72; p > 0.08 for WT versus TeNT and p < 0.0001 for TeNT^{sparse} versus WT or TeNT). The dashed blue line in (E) indicates significant correlation in WT retinas (p < 0.001), which was not observed for TeNT-expressing B6s.

See also Figures S2 and S3.

and precision to the known influences of activity on circuit development.

Supplemental Information

Supplemental Information includes Supplemental Experimental Procedures and four figures and can be found with this article online at <http://dx.doi.org/10.1016/j.cub.2014.08.018>.

Acknowledgments

We thank F. Soto, T. Holy, and P. Lukasiewicz for helpful comments on the manuscript and L. Zhao for excellent technical assistance. This research was made possible by support from the US NIH (EY 023341 and EY 021855), the Whitehall Foundation, the Mallinckrodt Foundation, the Sloan Foundation, and the Research to Prevent Blindness Foundation to D.K., as well as the Vision Core Grant (EY002687) to the Department of Ophthalmology and Visual Sciences at Washington University School of Medicine.

Received: February 26, 2014
Revised: July 11, 2014
Accepted: August 8, 2014
Published: September 11, 2014

References

- Felleman, D.J., and Van Essen, D.C. (1991). Distributed hierarchical processing in the primate cerebral cortex. *Cereb. Cortex* 1, 1–47.
- Sanes, J.R., and Zipursky, S.L. (2010). Design principles of insect and vertebrate visual systems. *Neuron* 66, 15–36.
- Antonini, A., Fagiolini, M., and Stryker, M.P. (1999). Anatomical correlates of functional plasticity in mouse visual cortex. *J. Neurosci.* 19, 4388–4406.
- Ben Fredj, N., Hammond, S., Otsuna, H., Chien, C.B., Burrone, J., and Meyer, M.P. (2010). Synaptic activity and activity-dependent competition regulates axon arbor maturation, growth arrest, and territory in the retinotectal projection. *J. Neurosci.* 30, 10939–10951.
- Buffelli, M., Burgess, R.W., Feng, G., Lobe, C.G., Lichtman, J.W., and Sanes, J.R. (2003). Genetic evidence that relative synaptic efficacy biases the outcome of synaptic competition. *Nature* 424, 430–434.
- Hua, J.Y., Smear, M.C., Baier, H., and Smith, S.J. (2005). Regulation of axon growth in vivo by activity-based competition. *Nature* 434, 1022–1026.
- Yasuda, M., Johnson-Venkatesh, E.M., Zhang, H., Parent, J.M., Sutton, M.A., and Umemori, H. (2011). Multiple forms of activity-dependent competition refine hippocampal circuits in vivo. *Neuron* 70, 1128–1142.
- Yu, C.R., Power, J., Barnea, G., O'Donnell, S., Brown, H.E., Osborne, J., Axel, R., and Gogos, J.A. (2004). Spontaneous neural activity is required for the establishment and maintenance of the olfactory sensory map. *Neuron* 42, 553–566.

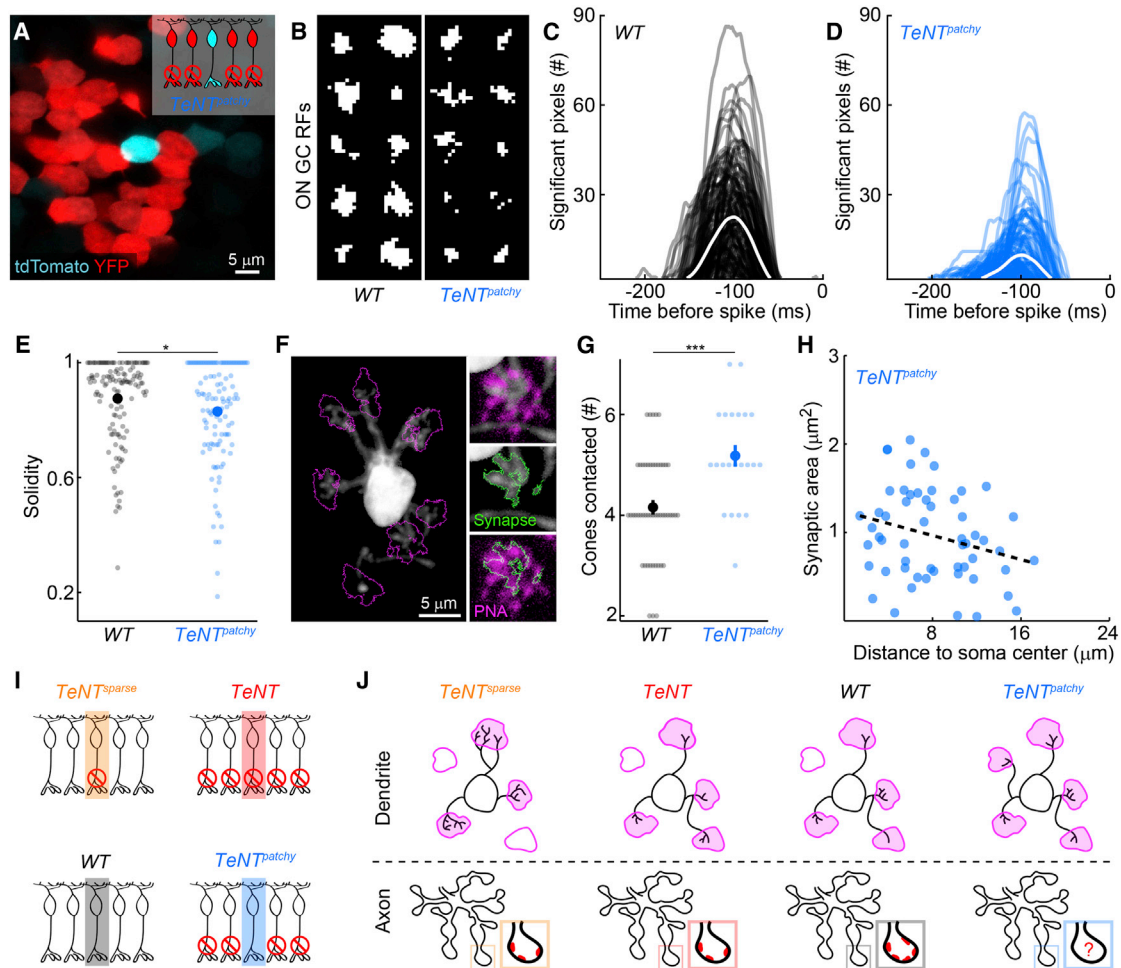


Figure 4. Dendrites of Active BCs with Silenced Neighbors Expand to Recruit More Cones

(A) Image of BC somata in a flat-mounted *TeNT^{patchy}* retina showing a single tdTomato-positive YFP-negative B6 surrounded by TeNT-expressing (YFP-positive) neighbors. The inset schematic illustrates labeling (cyan, tdTomato; red, YFP) and activity status of the analyzed B6 cells (middle cell) and their neighbors. Red circles with diagonal crossings indicate axonal silencing by TeNT expression.

(B) Binarized RF center maps of ten representative ON GCs recorded in *WT* (left) and *TeNT^{patchy}* (right) retinas. Spike-triggered averages (STAs) were constructed from GC responses to 1 hr of Gaussian checkerboard white-noise stimulation. Significant center pixels were defined as having higher intensity (ON GCs) at the temporal peak of the response than expected based on simulated STAs constructed by random placement of a similar number of spikes as the cell in question (Supplemental Experimental Procedures). The side length of each pixel in the RF maps is 28 μm .

(C and D) Plots of the STA time course of the number of significant ON pixels (i.e., significantly higher intensity than mean) of ON GCs indicate reduced RF center size but preserved response kinetics in *TeNT^{patchy}* (D; $n = 130$) compared to *WT* (C; $n = 134$) retinas.

(E) Comparison of the solidity of ON GC RFs in *WT* ($n = 134$) and *TeNT^{patchy}* ($n = 130$) retinas. Solidity was defined as the ratio of the area of the sum of the significant pixels over the area of the smallest convex polygon encompassing them. Each small circle represents one ON GC. Large circles (error bars) mark the population averages (\pm SEM).

(F) Projection through a confocal image stack of representative B6 dendrites in a *TeNT^{patchy}* retina. Insets show individual contacts of the B6 dendrite with cones stained with fluorescent PNA. Perimeters of cones and synaptic contacts are outlined in magenta and green, respectively.

(G) Comparison of the numbers of cones contacted by B6s in *WT* ($n = 51$) and *TeNT^{patchy}* ($n = 22$). Each small circle shows the number of cones contacted by one B6. Large circles (error bars) represent the population averages (\pm SEM). The increase in the number of cones contacted by B6s in *TeNT^{patchy}* retinas is mediated by an expansion of their dendritic territories (*WT*: $137 \pm 10 \mu\text{m}^2$, $n = 20$; *TeNT^{patchy}*: $197 \pm 14 \mu\text{m}^2$, $n = 15$; $p < 0.002$).

(H) Scatter plot of the area of cone-B6 synaptic contacts as a function of distance from the center of the B6 soma. Each circle represents the contacts of one cone with a B6 dendrite (*WT*: $0.74 \pm 0.05 \mu\text{m}^2$, $n = 87$; *TeNT^{patchy}*: $0.96 \pm 0.07 \mu\text{m}^2$, $n = 56$; $p < 0.01$). The dashed black line indicates significant correlation ($p < 0.02$).

(I) Schematic illustrating the activity status of the analyzed B6 cells (shaded areas) and their neighbors in *TeNT^{sparse}*, *TeNT*, *WT*, and *TeNT^{patchy}* mice. Red circles with diagonal crossings indicate axonal silencing by TeNT expression.

(J) Schematic summarizing the changes in bipolar development observed in *TeNT^{sparse}*, *TeNT*, *WT*, and *TeNT^{patchy}* mice. Changes in dendritic structure and connectivity with cones (magenta) are depicted in the top row, and effects on axonal morphology and the numbers of synapses (red) are illustrated in the bottom row.

See also Figure S4.

9. Masland, R.H. (2012). The neuronal organization of the retina. *Neuron* 76, 266–280.
10. Wässle, H., Puller, C., Müller, F., and Haverkamp, S. (2009). Cone contacts, mosaics, and territories of bipolar cells in the mouse retina. *J. Neurosci.* 29, 106–117.
11. Dunn, F.A., and Wong, R.O. (2012). Diverse strategies engaged in establishing stereotypic wiring patterns among neurons sharing a common input at the visual system's first synapse. *J. Neurosci.* 32, 10306–10317.
12. Morgan, J.L., Soto, F., Wong, R.O., and Kerschensteiner, D. (2011). Development of cell type-specific connectivity patterns of converging excitatory axons in the retina. *Neuron* 71, 1014–1021.
13. Schwartz, G.W., Okawa, H., Dunn, F.A., Morgan, J.L., Kerschensteiner, D., Wong, R.O., and Rieke, F. (2012). The spatial structure of a nonlinear receptive field. *Nat. Neurosci.* 15, 1572–1580.
14. Kerschensteiner, D., Morgan, J.L., Parker, E.D., Lewis, R.M., and Wong, R.O. (2009). Neurotransmission selectively regulates synapse formation in parallel circuits in vivo. *Nature* 460, 1016–1020.
15. Schiavo, G., Benfenati, F., Poulain, B., Rossetto, O., Polverino de Lauro, P., DasGupta, B.R., and Montecucco, C. (1992). Tetanus and botulinum-B neurotoxins block neurotransmitter release by proteolytic cleavage of synaptobrevin. *Nature* 359, 832–835.
16. Wurzig, K., Lichtenberger, T., and Hanitzsch, R. (2001). On-bipolar cells and depolarising third-order neurons as the origin of the ERG-b-wave in the RCS rat. *Vision Res.* 41, 1091–1101.
17. Schmitz, F., Königstorfer, A., and Südhof, T.C. (2000). RIBEYE, a component of synaptic ribbons: a protein's journey through evolution provides insight into synaptic ribbon function. *Neuron* 28, 857–872.
18. Jakobs, T.C., Koizumi, A., and Masland, R.H. (2008). The spatial distribution of glutamatergic inputs to dendrites of retinal ganglion cells. *J. Comp. Neurol.* 510, 221–236.
19. Morgan, J.L., Schubert, T., and Wong, R.O. (2008). Developmental patterning of glutamatergic synapses onto retinal ganglion cells. *Neural Dev.* 3, 8.
20. Okawa, H., Della Santina, L., Schwartz, G.W., Rieke, F., and Wong, R.O. (2014). Interplay of cell-autonomous and nonautonomous mechanisms tailors synaptic connectivity of converging axons in vivo. *Neuron* 82, 125–137.
21. Keeley, P.W., and Reese, B.E. (2010). Role of afferents in the differentiation of bipolar cells in the mouse retina. *J. Neurosci.* 30, 1677–1685.
22. Burrone, J., O'Byrne, M., and Murthy, V.N. (2002). Multiple forms of synaptic plasticity triggered by selective suppression of activity in individual neurons. *Nature* 420, 414–418.
23. Pozo, K., and Goda, Y. (2010). Unraveling mechanisms of homeostatic synaptic plasticity. *Neuron* 66, 337–351.
24. Turrigiano, G.G., and Nelson, S.B. (2004). Homeostatic plasticity in the developing nervous system. *Nat. Rev. Neurosci.* 5, 97–107.
25. Harrington, A.W., and Ginty, D.D. (2013). Long-distance retrograde neurotrophic factor signalling in neurons. *Nat. Rev. Neurosci.* 14, 177–187.
26. Pinheiro, P.S., and Mulle, C. (2008). Presynaptic glutamate receptors: physiological functions and mechanisms of action. *Nat. Rev. Neurosci.* 9, 423–436.
27. Du, J.L., Wei, H.P., Wang, Z.R., Wong, S.T., and Poo, M.M. (2009). Long-range retrograde spread of LTP and LTD from optic tectum to retina. *Proc. Natl. Acad. Sci. USA* 106, 18890–18896.
28. Bleckert, A., and Wong, R.O. (2011). Identifying roles for neurotransmission in circuit assembly: insights gained from multiple model systems and experimental approaches. *Bioessays* 33, 61–72.